Acta Geodyn. Geomater., Vol. 21, No. 1 (213), 111–120, 2024
DOI: 10.13168/AGG.2024.0010
journal homepage: https://www.irsm.cas.cz/acta

ORIGINAL PAPER

IDENTIFYING THE GEOLOGICAL STRUCTURE OF THE GARYAN AREA IN NORTHWEST LIBYA USING EIGEN-6C4 SATELLITE GRAVITY DATA

Fouzie TREPIL [1, 2], Nordiana Mohd MUZTAZA [1] *, Ismail Ahmad ABIR [1], Mohamed A. SALEEM [3], Khiri Abubaker KHALF [1] and Syarawi Muhammad SHARONI [1]

[1] *School of Physics, Universiti Sains Malaysia 11800, Pulau Penang, Malaysia*
[2] *Geophysics Dept., Faculty of Science, University of Tripoli, PO Box 13275, Tripoli, Libya*
[3] *Petroleum Institute (LPI), Tripoli, 6431, Libya*

**Corresponding author's e-mail:* mmnordiana@usm.my

ARTICLE INFO

Article history:
Received 18 January 2024
Accepted 5 March 2024
Available online 2 April 2024

Keywords:
Geological structure
Satellite gravity data
EIGEN-6C4
Garyan
Libya

ABSTRACT

Satellite gravity data can be used in this study to characterise hitherto unexplored regions and enhance scientific understanding of the studied area. However, the geological ambiguity of the study area makes it challenging to figure out the geological interpretation within and around the area. Therefore, this work focused on the Garyan area in the northwest part of Libya for the purpose of identifying geological structures. The Garyan region is a part of Jabal Nafusah (central Jabal) due to its geographic location and the character of the escarpment. The gravity data was analysed, designed, and developed into a geophysical model using the Oasis Montaj programme. Several analytic techniques are applied to gravity datasets for subsurface structure investigation, including (TDR) tilt derivative, (THG) total horizontal gradient, (PS) Power spectrum technique, (AS) Analytical signal, and (ED) Euler deconvolution. The results identified the presence of faults trending in different orientations (N-S, NW-SE, E-W, NNW-SSE, NE-SW), with source depths ranging between 300 and 2300 m, which indicates a complex tectonic history in the area. Clearly, this work will reduce the ambiguity of geological interpretations and provide better information on the dominant trends for future exploration activities in the study region. It also detects the contacts of density variation and estimates the depth of the gravity sources from satellite-EIGEN-6C4 gravity data.

1. INTRODUCTION

Mapping structural features is essential to exploring hydrocarbon, geothermal, groundwater, and mineral resources. More so, understanding the rock units, faults, contacts, dykes, and lineaments is significant to the structural study (Abdulkadir et al., 2022). Satellite gravity data analysis is constructive in primary exploration, especially in studying geological conditions in remote and extended areas (Kurniawan, 2012; Sadeghi et al., 2013; Zeinelabbdein et al., 2014). The study region (Fig. 1) is in northwest Libya's Jabel Nafusah escarpment. It's between 12.91 and 13.11 degrees east and 32.13 and 32.34 degrees north, between the Ghadamis and Jafarah basins. Because the study area lies between the Ghadames and Pelagian-producing basins, it is suitable for potential hydrocarbon accumulation. The area is also considered to be a structurally complex region of the fold belt of the Atlas, formed as a result of tectonic plate collisions and subsequent folding and uplifting of the Earth's crust (Trepil et al., 2021). Numerous geological and geophysical investigations have been conducted in the Garyan region and adjacent area northwest of Libya, including gravity, magnetics, and remote sensing data to understand the surface and subsurface structures (Desio et al., 1963; Christie, 1966; Steckler et al., 1988; Swire and Gashgesh, 2000; Saadi et al., 2009; Alfandi, 2012). Steckler et al. (1988) indicated that the area of study is part of the rift's flank, or the footwall. During rifting, such regions frequently uplift. Alfandi (2012) reported that the region's tectonic activity has been relatively quiescent (Mid-Late Triassic). The major Aziziyah fault in the north and perhaps further inland in the south are associated with active tectonics within the continental interior. Saadi et al. (2009) used DEM, Landsat, geological maps, and aeromagnetic data to constrain the geological structure in the Jafarah Plain and around Jabel Nafusah, which includes Garyan. Trepil et al. (2021) utilised aeromagnetic and land gravity data to investigate the Jafarah plain and its neighbouring Jabal Nafusah. However, numerous geoscientific datasets are available in the region of study that haven't been extensively analysed or published in scientific research and are interpreted structurally (Saadi et al., 2011). The geological ambiguity of the study region makes it challenging to figure out the geological structures within and around the area. Unfortunately, our understanding of structural development is heretofore insufficient. With

Cite this article as: Trepil F, Muztaza NM, Abir IA, Saleem MA, Khalf KA, Sharoni SM: Identifying the geological structure of the Garyan area in northwest Libya using eigen-6c4 satellite gravity data. Acta Geodyn. Geomater., 21, No. 1 (213), 111–120, 2024. DOI: 10.13168/AGG.2024.0010

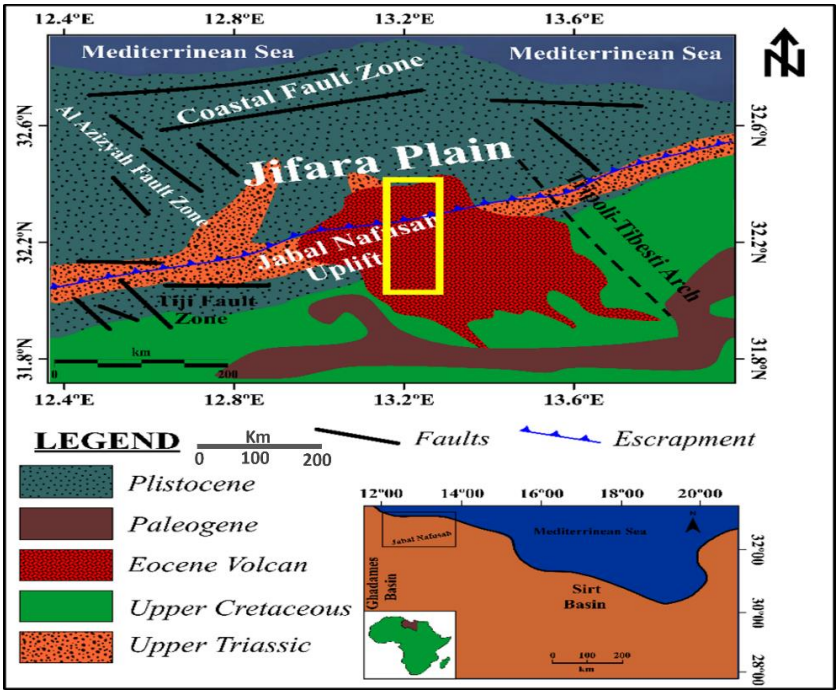

Fig. 1 Location map (yellow rectangular) and a simplified geological map of the area modified after Zivanovic (1977).

the Oasis Montaj programme, many filters are used to interpret gravity data. Therefore, the investigation of geological structures provides significant insights into the history and development of the study region and the surrounding region, which are required for potential hydrocarbon exploration activities (Saadi et al., 2011). Consequently, this study utilises gravity data to identify geological structures that exist in the Garyan region of northwest Libya. Furthermore, the main results are useful for identifying new features that facilitate a deeper understanding of the geological structures in the Garyan area.

2. GEOLOGICAL SETTING

The Garyan region is a part of the Jabel Nafusah due to its geographical location and the escarpment's characteristics (Fatmi et al., 1978). The Nafusah Uplift (also called the "Nafusah Arch"), shown in Figure 1 (Abohajar et al. 2009), is a major tectonic feature that extends from east to west and from northeast to southwest, which is the boundary between the Ghadames Basin in the north and the plain of Jifara (Trepil et al., 2021). According to Abdunaser and McCaffrey (2015), the Nafusah Arc formed a thick succession of Paleozoic deposits as a portion of the Ghadames basin during the lower Paleozoic. According to Miller (1971) and Giraudi (2005), the Nafusah Arc is among the most distinctive morphological features in northwest Libya. Basins within northwest Africa developed as the result of a phanerozoic sequence of uplifts that intersected each other in diagonal directions; furthermore, the Early Caledonian tectonic phase revitalised what was previously a weak suture zone with Pan-African origins (Klitzsch, 1970; Klitzsch and Gray, 1971). Accordingly, it appears that this is the origin of the common idea that uplifting is a part of the predominantly E-W trending "Nafusah arch." Farahat et al. (2006) concluded that large recent continental landmasses are frequently affected by neotectonic activity; this is typically related to mantle events during which uplift is created through rising plumes related to hot spots (Alfandi, 2012). According to Goudarzi (1970), the Garyan-Yafran Arch, which is the major structural lineament, is a large anticlinal swell that trends northwest to southeast. In the upper Cretaceous or lower Tertiary, the Garyan-Tarhunah strip was uplifted, yielding an NW-SE trending anticlinal swelling (Saadi et al., 2008). Jabal Nefusa was considered to have been uplifted during the Hercynian orogenesis by Burollet (1963). The uplift, according to Lipparini (1968), was associated with northwest-southeast faulting. In general, the Garyan area (Anketell and Gjellali, 1991) consists of clastic and carbonate rocks (Mesozoic deposits such as limestone, which is combined with shale and sandstone). Volcanic activities that accrued during the late Cretaceous period generated volcanic rocks that formed and had an impact on the Upper Jurassic deposits (Hallett and Clark-Lowes, 2017). Basalt cones, basalt flows, and phonolite intrusions are the three main forms of volcanic rocks in the region (Antonovic, 1977). According to Abdunaser and McCaffrey (2015), the tectonic movements in the Eocene created basaltic flows within the Garyan area.

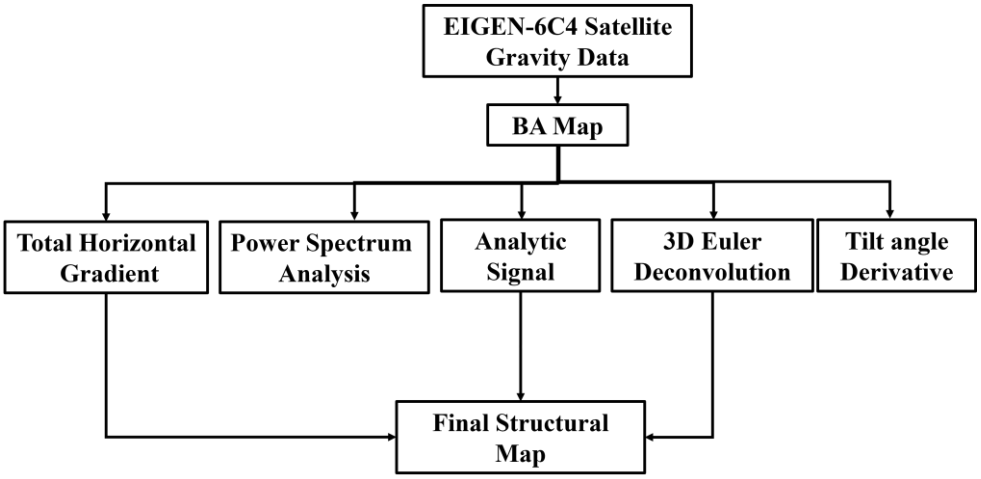

Fig. 2 Methodology flowchart.

3. MATERIALS AND METHOD

3.1. GRAVITY DATA

The EIGEN-6C4 satellite gravity dataset for the Garyan area was provided by the ICGEM (International Centre for Global Earth Modelling) website. (Pal and Majumdar, 2015; Tedla et al., 2011) reported that EIGEN-6C4 satellite gravity datasets are particularly appropriate for studying long wavelength characteristics that could be lost via ground gravity measurement, and they provide global coverage that is unaffected by the terrain's roughness and inaccessibility (Kumar et al., 2022). Satellite gravity data analysis is one of the exploration methods that can be used to outline the subsurface structures in this study. (Kurniawan, 2012) highlights that this method has advanced in recent years. Satellite gravity interpretation has several applications in primary investigation research due to its inexpensive cost and its ability to study geological conditions in remote and/or extended areas (Darisma et al., 2019). Numerous scientists have applied satellite gravity data, e.g., Trung et al. (2004) have used gravity datasets to delineate the main tectonic elements within the South China Sea. Also, Tedla et al. (2011) created a map of Africa's crustal thickness estimate using data from a global gravity model. More so, other researchers, such as Pal et al. (2016) and Narayan et al. (2017), have utilised the EIGEN-6C4 and other global combined gravity field model data for structural mapping in the context of the 85°E Ridge and its environs. The gravity dataset is made up of 462 gravity data points and a grid with an interval of 0.01º x 0.01º, approximately 1 km, the maximum resolution for the EIGEN-6C4.

3.2. GRAVITY DATA PROCESSING

Originally, the satellite gravity dataset was provided as the FAA (Free Air Anomaly). Thus, the dataset should be corrected to remove the effect of the rock mass between the measuring station and the mean sea level. The result of performing all appropriate corrections on the gravity dataset is the Bouguer gravity anomaly. Further, the gravity dataset was gridded utilising minimal curvature random gridding to produce the Bouguer anomaly grid. The Bouguer anomaly (Fig. 3) in gravity data, however, includes various anomalies with a wide range of amplitudes. The resulting Bouguer anomaly grid provides a representation of the gravity anomalies that are primarily associated with subsurface density variations, while accounting for the effects of topographic masses. This grid can be further analyzed to identify geological structures, delineate subsurface features, or understand the distribution of mass within the Earth's crust. EIGEN-6C4 satellite gravity data is processed using total horizontal gradient analysis, power spectrum analysis, analytical signal, tilt derivative, and Euler deconvolution. In Figure 2, we see a simplified flowchart of the methodology.

- **Total Horizontal Gradient (THG)**

Using upright contacts, the THG equation (1) indicates the boundaries of the gravity anomalies. It is anticipated that the geologic contacts in the study region will be more easily discernible after being filtered using the horizontal gradient. The THG approach (Cordell, 1979) can be used to detect density variation contacts in gravity data.

$$\mathrm{HG}(x,y) = \sqrt{\left(\frac{\partial G}{\partial x}\right)^2 + \left(\frac{\partial G}{\partial y}\right)^2} \quad (1)$$

Where G represents the gravity anomaly, The strength of a horizontal gradient at the specific location (x,y) is represented by HG(x,y). It is calculated based on the partial derivatives (∂G/∂x and ∂G/∂y) of the gravity anomaly towards x and y.

- **Power spectrum analysis**

Power spectrum analysis represents one of the most common methods to figure out the depth of gravity sources (Spector and Grant, 1970). The gravity maps' power spectrum is the product of their 2D Fourier transform and complex conjugate (Ghazala et al., 2018). The average depth of the gravity source can

be related to specific features in the radially averaged power spectrum. Different frequencies in the power spectrum may correspond to different depths of the subsurface structures contributing to the gravity signal. Thus, an average depth associated with the gravity sources equation (2) is determined after using the information derived from the 2-D radially averaged power spectrum and possibly other data from equation (Spector and Grant, 1970).

$$H = -\frac{S}{4\pi} \quad (2)$$

The depth (H) represents the depth of the subsurface structure being investigated, and the slope (S) of the log energy spectrum refers to the rate at which the logarithm of the power values changes with frequency.

- **Analytical Signal (AS)**

The analytic signal is a mathematical technique used to enhance and analyze gravity data. It is particularly useful in the interpretation of Bouguer gravity anomalies, it estimated the sources are distinct dipping contacts between vast geological sections (El-Ata et al., 2013). Moreover, it is only moderately sensitive to data noise and interference from adjacent sources. The analytic signal technique assumed that gravity contacts as causative sources. The analytical signal method equation (3) (Nabighian, 1972), commonly also known as the total gradient or analytic signal amplitude, has been widely used, with improvements and investigations conducted to enhance its effectiveness and explore its applications in various geological settings since its inception (Saibi et al., 2016).

$$|A(x,y)| = \sqrt{\left(\frac{\partial G}{\partial x}\right)^2 + \left(\frac{\partial G}{\partial y}\right)^2 + \left(\frac{\partial G}{\partial z}\right)^2} \quad (3)$$

Where G represents the anomalous gravity field, (∂G/∂x and ∂G/∂y) refer to its horizontal derivatives, and ∂G/∂z refers to its vertical derivative.

- **Tilt angle derivative (TDR)**

Miller and Singh (1994) and Verduzco et al. (2004) proposed the analytic signal approach, which was refined by the TDR tilt derivative method equation (4), also known as the tilt angle method, as a technique utilized to sharpen and enhance gravity anomalies. It utilizes the second vertical derivative of the anomaly to determine the tilt angle of the field. The TRD tilt angle can be utilized for estimating the depth and position of the anomalous sources. The method assumes that the sources are approximated as two-dimensional structures. The TDR is a technique used to discriminate between gravity anomalies by analyzing their derivatives, which are vertical and horizontal derivatives (Ming et al., 2021). When the TAD value is positive, it shows a positive contrast with the underlying causative source, whereas when it is negative, it indicates that it is outside the limits of the source.

$$\text{TDR} = \tan^{-1}\left\{\frac{\frac{\partial G}{\partial z}}{\sqrt{\left(\frac{\partial G}{\partial x}\right)^2 + \left(\frac{\partial G}{\partial y}\right)^2}}\right\} \quad (4)$$

Where the observed gravity field G is at a given location (x, y). (∂G/∂x) and (∂G/∂y) denote the horizontal derivative. (∂G/∂z) signifies the vertical derivative of the gravity field.

- **Euler deconvolution**

Euler deconvolution estimates source depth and location for various homogeneous gravity sources. A structural index is an exponential variable that explains the nature of the geologic bodies, as shown in (Table 1). This technique is particularly helpful in interpreting gravity data because it involves such little basic knowledge about the source body's structure (Reid et al., 1990; Thompson, 1982). The Euler deconvolution expression in three dimensions is as follows:

$$N(B-G) = (x-x_0)\left(\frac{\partial G}{\partial x}\right) + (y-y_0)\left(\frac{\partial G}{\partial y}\right) + \\ +(z-z_0)\left(\frac{\partial G}{\partial z}\right) \quad (5)$$

Where G describes the gravity field generated by causative bodies at a specific location (x, y, and z) in terms of the coordinates of the source site ($x_0, y_0,$ and z_0), the baseline level of the field (B), and the structural index or homogeneity degree (N).

4. RESULTS AND DISCUSSION

The Bouguer anomaly map for the region under investigation is shown in Figure 3. The BA exhibits amplitude anomalies ranging from -18 to 6 mGal. The trending directions of anomalies (NW-SE, N-S, E-W, and NNW-SSE) can be associated with various geological structures. The high positive anomaly values of 6 mGal found in the southwest (H3), northeast (H1), and central parts of the study region (H2) suggest that these areas have a stronger gravitational field than the surrounding areas. Positive anomalies indicate areas with greater gravitational attraction, which can be associated with regions of higher-density rocks or deeper crustal structures. This strong positive gravity anomaly value is associated with Cenozoic volcanic rock in the area with a high density that formed during the Eocene. The lowest values (-18 mGal) of BA are indicated in the study area's central part (L1) and the southern part (L2). These lower gravity values are most likely due to the existence of sediments with high thicknesses in

Table 1 Structural index for magnetic (FitzGerald et al., 2004).

Source	Gravity
Sphere	2
Horizontal	1
Fault	0

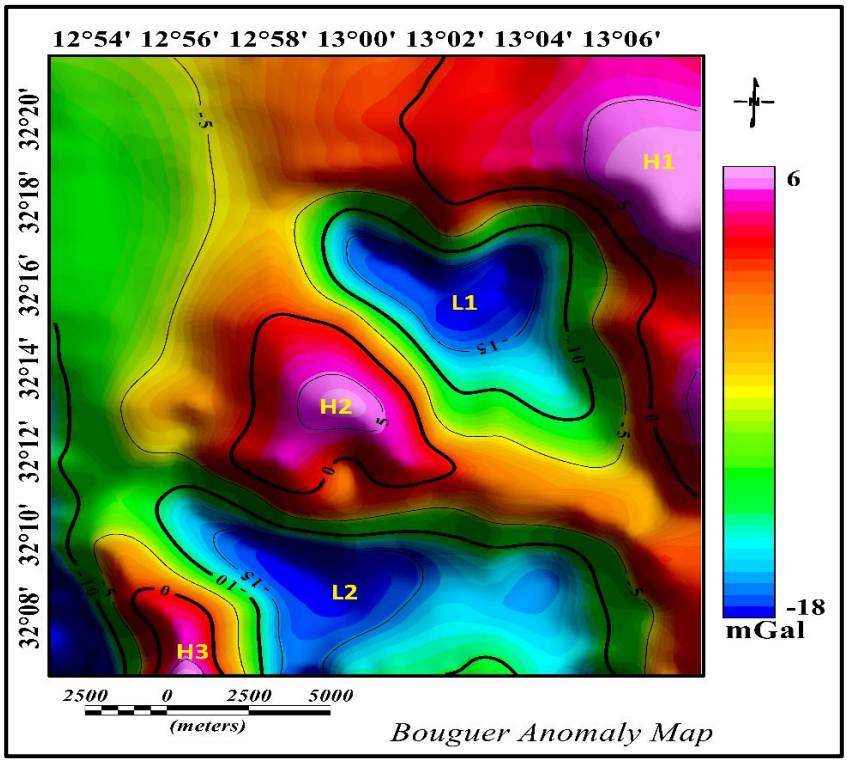

Fig. 3 Bouguer anomaly map (BA) within the study region.

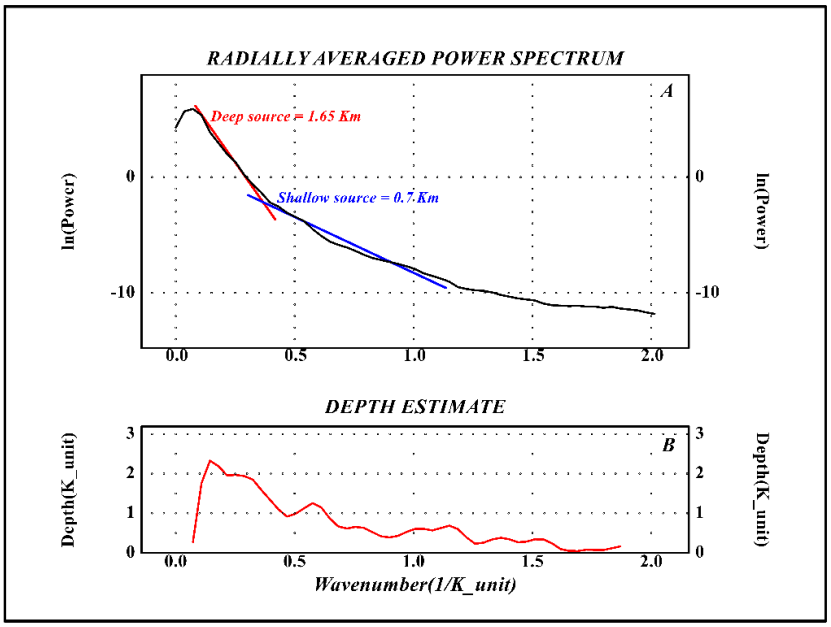

Fig. 4 (A) Radially average energy spectrum of the Garyan region's gravity anomaly; (B) Depth estimation of gravity source.

various regions. Additionally, negative anomalies represent regions that have decreased gravitational attraction, which could be associated with grabens that developed in the NW-SE along marginal segments of the Jurassic/Triassic-Jurassic uplifts.

In this study, (Fig. 4A) exhibits the energy power spectrum of the gravity dataset, whereas (Fig. 4B) reveals the estimated depth of the gravity sources. Two various gravity sources are observable: the deep source at an approximate depth of 1.65 kilometres and a shallower source at a depth of about 0.7 kilometres from the next equation: H = -S/4. Where H is the depth and S is the slope of the log (energy) spectrum.

The result shows a strong positive amplitude peak of the THG (Fig. 5) that delineates the subsurface elements of the study region as trends NNW-SSE, NE-SW, NW-SE, N-S, and E-W, which are referring to the result of various tectonic movements, such as

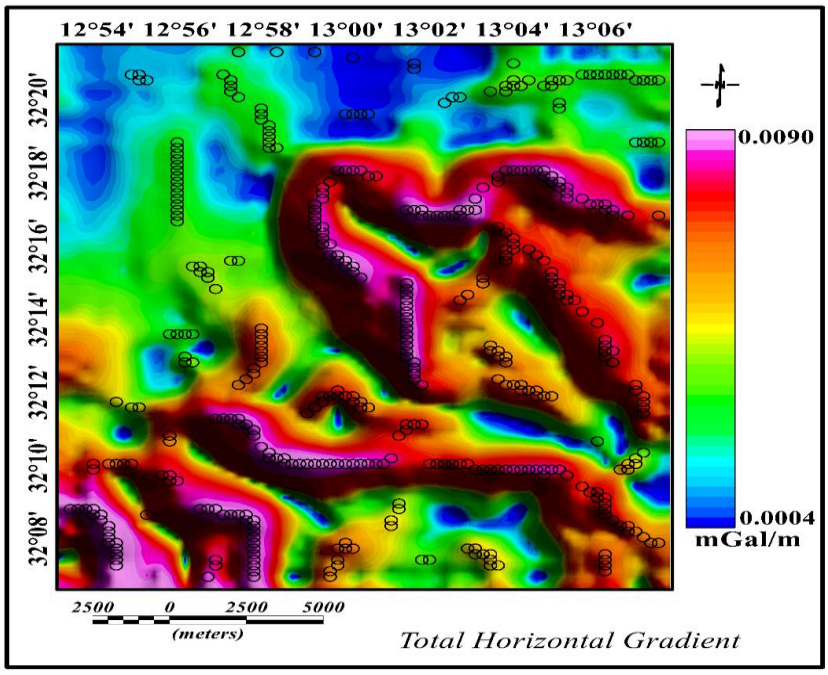

Fig. 5 Map resulting from applying the THG technique, the black circles represent the maximum of the horizontal gradient, where contacts could be located.

a tectonic activity in the Caledonian and then Hercynian, that cut Mesozoic sedimentary sequence and are the origin of the commonly held belief that the Nafusah uplift is a feature of a "Nafusah arch" that trends mostly east to west. The main fault trend is NW-SE, which may be associated with the collision of the African and European in the Hercynian event, which is intersected by subordinate trending faults E-W, which run parallel to the Jabel Nafusah. The E-W fault trend is linked to the widely held belief that the Jabel Nafusah uplift formed part of an essentially E-W trending "Nafusah arch" during the early Caledonian age, whereas the N-S trending fault associated with structural development in the NW African basin was periodically reactivated as strike-slip faults that occurred in the early Caledonian and Hercynian tectonic events, according to Klitzsch (1970), and may be due to the similar tectonic event that caused the Nafusah Arc. This NE-SW trend was most probably influenced by the well-developed NNE-SSW structures of Paleozoic rocks associated with the Tibesti-Sirte Uplift. The NNW-SSE fault trend is related to the reactivation of Cretaceous lineaments in the Hun Graben in the Caledonian age.

The analytical signal technique is utilised for the Bouguer anomaly (Fig. 6). An analytical signal map of a region indicates the high gravity anomalies bordered by fault trends NE-SW, NW-SE, E-W, and N-S, which refer to the intrusive and extrusive volcanic rocks that occurred within this region during the upper Cretaceous or lower Tertiary. The maxima of the AS are used to identify the subsurface structures. The high values that appear in the southwest and central parts of the map are reflected in the high amplitude of the analytic signal peaks for gravity data, showing that all these areas contain significant variations in gravity density that form identifiable features on this map. Circles identify locations of the Analytic signal maxima where gravity anomalies are most prominent. The peaks represent areas where the strength of the gravity field deviates significantly from the background or regional gravity field. These peaks serve as indicators of the boundaries or edges of gravity sources.

The Bouguer anomaly in Oasis Montaj is utilized to create Euler deconvolution maps. Various values (0, 1 and 2) were set to the structural index in order to figure out the best solutions that could be achieved. Furthermore, structural index = 0 yields superior solutions compared to SI = 1 and SI = 2, since these data are clustered in a few key locations rather than being randomly distributed across the study region. In addition, the solution of structural index =0 provides the main faults superimposed on the zero contour of TDR. The window size of 5x5 and the solution with a structural index of 0 for a maximum depth tolerance of 10 % indicate the best possible clustering of source-depth solutions. A Euler deconvolution of the Bouguer anomaly (Fig. 7) demonstrates that its depth varies from 300 m to 2300 m with an E-W, NNW-SSE, NE-SW, N-S, and NW-SE trend. The N-S and NW-SE trends are commonly found along the eastern and central parts of the study area. The NNW-SSE trend is identified in different areas of the region. The E-W trend is mostly located in the southern area of the region. The fault trend that is oriented in the NE-SW direction is observed in the northwestern part of the area. The Euler solution map confirmed the trend faults observed in the THG, AS, and TDR.

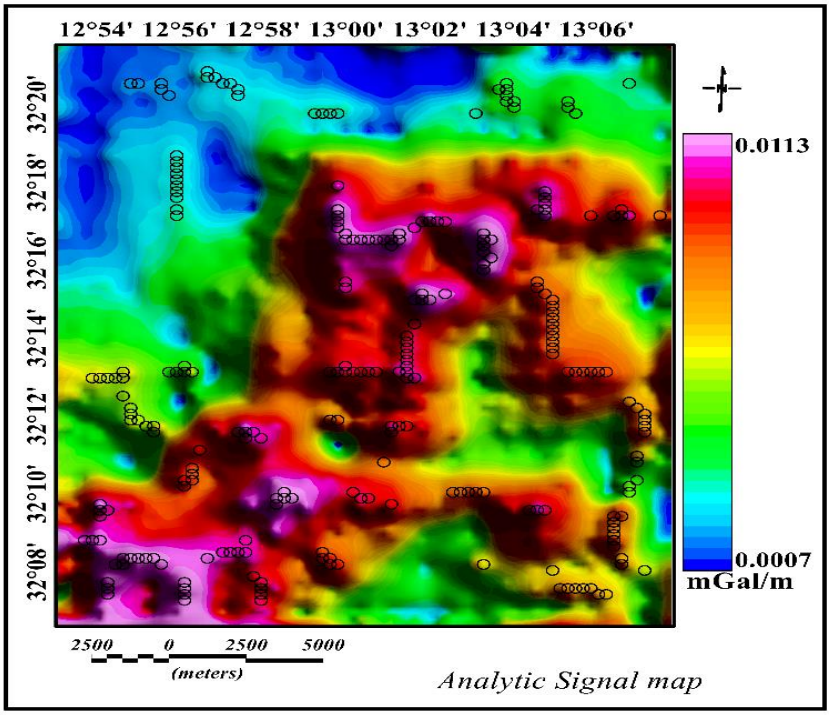

Fig. 6 Analytic signal map of BA.

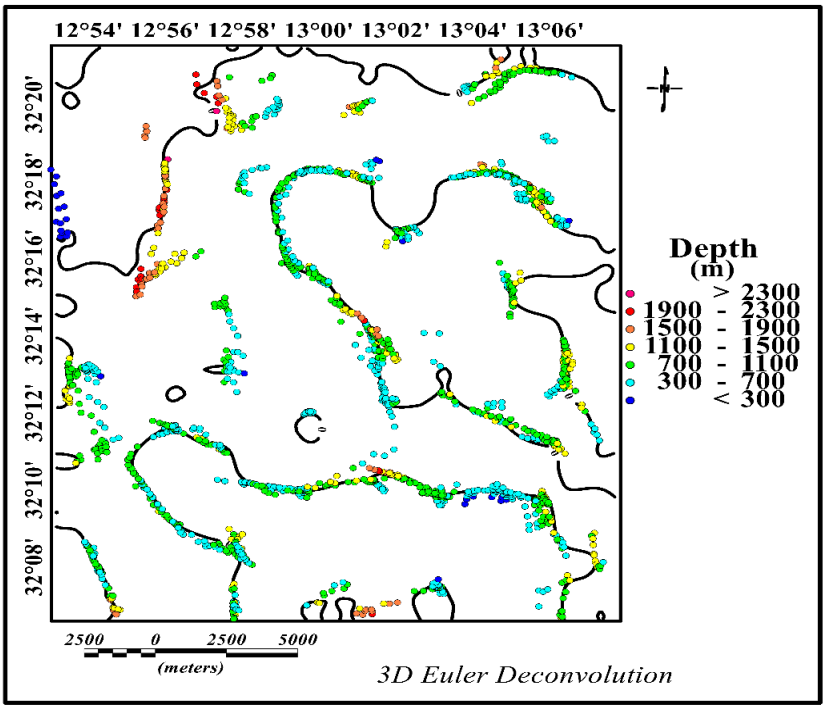

Fig. 7 3D Euler deconvolution map (W= 5, SI= 0).

A tilt derivative is particularly advantageous because it can reveal the zero-contour line that appears on or near a contact between different geological units or structures. TDR filters frequently tend to locate anomalies over their sources. The TDR of the Bouguer anomaly (Fig. 8) indicates fault trends with positive contrast. These fault trends predominantly occur in the northwest-southeast (NW-SE), east-west (E-W), and north-northwest-south-southeast (NNW-SSE) directions. The TDR map shows anomalies with magnitudes ranging from -1.32 to 1.31 degrees. Near the edges of the source, the TDR value is approximately zero. When the TAD value is positive, it shows a positive contrast with the underlying causative source, whereas when it is negative, it indicates that it is outside the limits of the source.

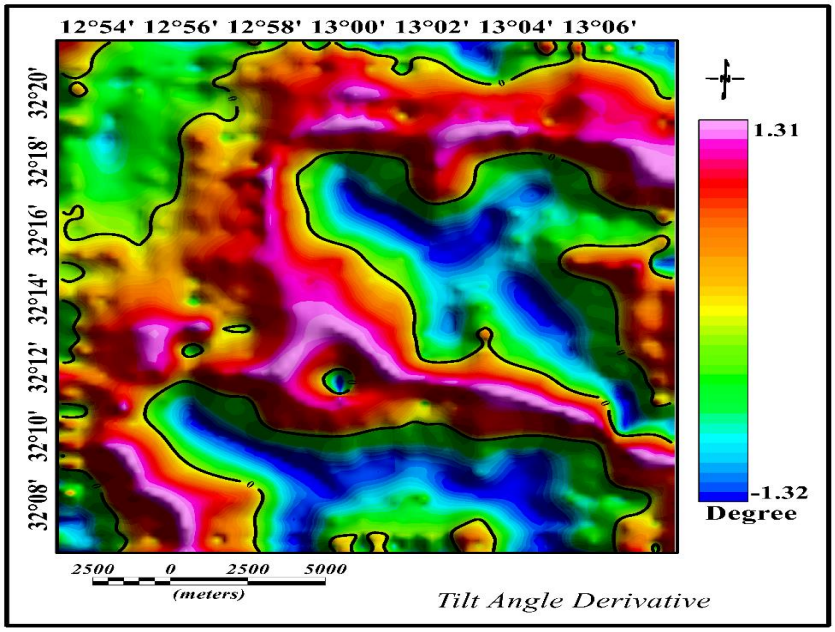

Fig. 8 Derivative of the tilt angle.

The structural map and a rose diagram of the Garyan region (Fig. 9) The structural map shows different trends of faults, while the rose diagram provides information about the orientations or trends of these faults. The structural map depicts the distribution and arrangement of geological structures, including faults, within the Garyan region. The different trend faults from the NNW-SSE, NW-SE, N-S, NE-SW, and E-W are represented and labelled on the structural map, indicating their locations within the region. The rose diagram, on the other hand, is a graphical representation used to display the frequency or distribution of orientations or trends of geological features such as faults. Thus, the diagram provides a concise summary of the predominant fault orientations within the region. The final structural map is constructed by combining the prominent trends identified from AS, THG, and Euler of the BA grid. These faults represented different tectonic activities during the Caledonian and Hercynian ages.

5. CONCLUSION

Various analytical techniques, such as total horizontal gradient, power spectrum, analytical signal, Euler deconvolution, and tilt derivative, are applied to the BA dataset to identify the subsurface structure elements of the Garyan regions of NW Libya. The Bouguer anomaly map demonstrates that the study region has anomaly values that range from -18 to 6 mGal. The various trends of faults were found in the N-S, NW-SE, E-W, NNW-SSE, and NE-SW directions, and they were assumed to be the results of tectonic activity in the Cenozoic period and tectonic movements of the Hercynian and Caledonian. The Euler deconvolution of the BA grid indicated that the source depth ranges between 300 m and 2300 m. All these findings of faults are associated with the tectonic features of the area. Consequently, identifying these faults is important to reduce the ambiguity of geological interpretations and provide more information on the dominant trends for future exploration activities in the study region.

ACKNOWLEDGEMENTS

Acknowledgement to the Ministry of Higher Education Malaysia for the Fundamental Research Grant Scheme with Project Code: FRGS/1/2022/STG08/USM/03/1 entitles "Performance-Based Multimodal Geophysical Design for Soil Dynamic Properties to Improve Visualization of Subsurface Conditions" and also a research university grant entitles "Integrated geophysical characterization of geothermal exploration and strategy for the sustainable use of geothermal resources" with account no. 1001/PFIZIK/8011110.

REFERENCES

Abdulkadir, Y.A., Fisseha, S. and Jothimani, M.: 2022, Digital elevation model and satellite gravity anomalies and its correlation with geologic structures at Borena basin, in the Southern Main Ethiopian Rift. Eur. J. Remote Sens., 55, 1, 540–550. DOI: 10.1080/22797254.2022.2130096

Abdunaser, K. and McCaffrey, K.: 2015, A new structural interpretation relating NW Libya to the Hun Graben, western Sirt Basin based on a new paleostress inversion. J. Earth Syst. Sci., 124, 8, 1745–1763. DOI:10.1007/s12040-015-0631-4

Abohajar, A., Krooss, B., Harouda, M. and Littke, R.: 2009, Maturity and source-rock potential of Mesozoic and Palaeozoic sediments, Jifarah Basin, NW Libya. J. Pet. Geol., 32, 4, 327–341. DOI: 10.1111/j.1747-5457.2009. 00453.x

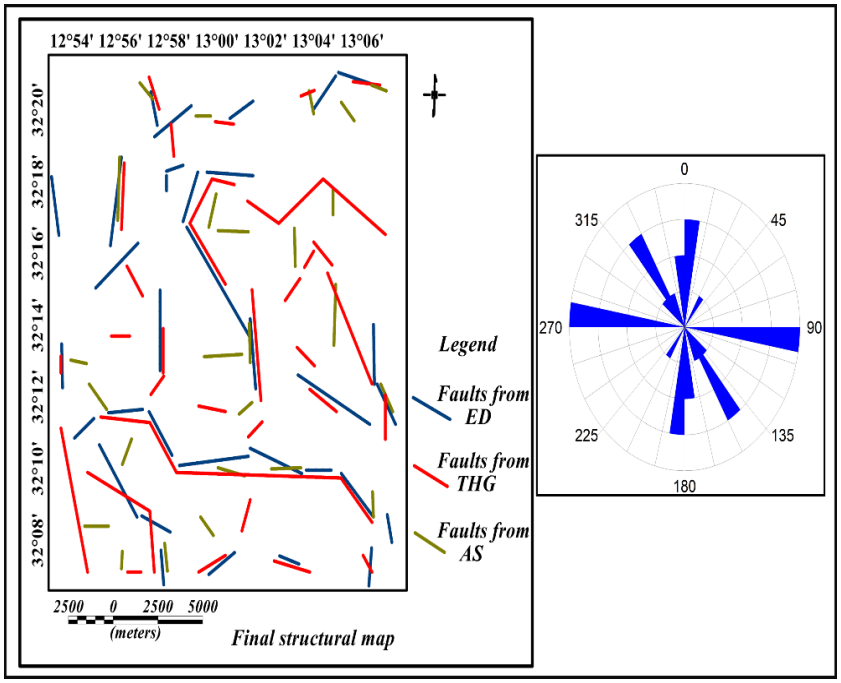

Fig. 9 Structure map of the Garyan area and a rose diagram of extracted faults from the THG, AS, TDR, and Euler deconvolution.

Alfandi, E.: 2012, Early Mesozoic stratigraphy, sedimentology and structure of the Gharian area, north-western Libya. Ph.D Thesis, University of Plymouth. DOI: 10.24382/3376

Anketell, J. and Gjellali, S.: 1991, A palaeogeologic map of the Pre-Tertiary surface in the region of the Jifarah Plain and its implication to the structural history of Northern Libya. In: Salem, M.J., Busrewil, M.T. and Ben Ashour, A.M., Eds., Geology of Libya, 7, Elsevier, Amsterdam, 2681–2687.

Antonovic, A.: 1977, Geological map of Libya 1/250 000, Mizdah. Industrial Research Centre, Tripoli, Socialist People's Libyan Arab Jamahiriyah, sheet NH, 33–31.

Burollet.: 1963, Excursion to Jebel Nefusa. Petroleum Exploration Society of Libya, Tripoli.

Christie, A.M.: 1966, Geology of the Garian Area, Tripolitania, Libya. Geological section, Ministry of Industry. Bull. 5, 64 pp.

Cordell, L.: 1979, Gravimetric expression of graben faulting in Santa Fe Country and the Espanola Basin, New Mexico. Paper presented at the New Mexico Geological Society. Guidebook: 30th Field Conference, New Mexico, 59–64.

Darisma, D., Marwan, M. and Ismail, N.: 2019, Geological structure analysis of satellit gravity data in oil and gas prospect area of West Aceh-Indonesia. J. Aceh Phys. Soc., 8, 1, 1–5. DOI:10.24815/jacps. v8i1.12750

Desio, A., Ronchetti, R.C., Pozzi, R., Clerici, F., Invernizzi, G., Pisoni, C. and Vigano, P.L.: 1963, Stratigraphic studies in the Tripolitanian Jebel (Libya). Mem. Riv. Ital. Paleontol. Stratigr., 9, 126 p.

El-Ata, A.S.A., EI-Khafeef, A.A., Ghoneimi, A.E., Abd Alnabi, S.H. and Al-Badani, M.A.: 2013, Applications of aeromagnetic data to detect the basement tectonics of Eastern Yemen region. Egypt. J. Pet., 22, 2, 277–292. DOI: 10.1016/j.ejpe.2013.06.007

Farahat, E., Ghani, M.A., Aboazom, A. and Asran, A.: 2006, Mineral chemistry of Al Haruj low-volcanicity rift basalts, Libya: implications for petrogenetic and geotectonic evolution. J. African Earth Sci., 45, 2, 198–212. DOI: 10.1016/j.jafrearsci.2006.02.007

Fatmi, A.N., Sbeta, A.M. and Eliagoubi, B.A.: 1978, Guide to the Mesozoic stratigraphy of Jabal Nefusa, Libyan Jamahiriya. Arab Development Institute. Publication No. 7, 35 pp.

FitzGerald, D., Reid, A. and McInerney, P.: 2004, New discrimination techniques for Euler deconvolution. Comput. Geosci, 30, 5, 467–469. DOI: 10.1016/j.cageo.2004.03.006

Ghazala, H.H., Ibraheem, I.M., Lamees, M. and Haggag, M.: 2018, Structural study using 2D modeling of the potential field data and GIS technique in Sohag Governorate and its surroundings, Upper Egypt. NRIAG J. Astron. Geophys., 7, 2, 334–346. DOI: 10.1016/j.nrjag.2018.05.008

Giraudi, C.: 2005, Eolian sand in peridesert northwestern Libya and implications for Late Pleistocene and Holocene Sahara expansions. Palaeogeogr. Palaeoclimatol. Palaeoecol., 218, 1-2, 161–173. DOI: 10.1016/j.palaeo.2004.12.014

Goudarzi, G.H.: 1970, Geology and mineral resources of Libya–a reconnaissance. Geol. Surv. Prof. Pap., 660., 1–112. DOI:10.3133/PP660

Hallett, D. and Clark–Lowes, D.: 2017, Petroleum geology of Libya, Elsevier.

Klitzsch, E.: 1970, The structural history of the Central Sahara: New insights into the structure and palaeogeography of a plateau. Geol. Rev., 59, 459–527.

Klitzsch, E. and Gray, C.: 1971, The structural development of parts of North Africa since Cambrian time. Paper presented at the Symposium on the geology of Libya: Tripoli, Faculty of Sciences, University of Libya, 256–260.

Kumar, S., Pal, S.K., Guha, A., Sahoo, S.D. and Mukherjee, A.: 2022, New insights on Kimberlite emplacement around the Bundelkhand Craton using integrated satellite–based remote sensing, gravity and magnetic data. Geocarto Int., 37, 4, 999–1021. DOI: 10.1080/10106049.2020.1756459

Kurniawan, F. A.: 2012, Pemanfaatan Data Anomali Gravitasi Citra GEOSAT dan ERS–1 Satellite untuk Memodelkan Struktur Geologi Cekungan Bentarsari Brebes. Indones. J. Appl. Phys., 2, 2, 1–14, (in Indonesian).

Lipparini, T.: 1968, Tectonics and Geomorphology, Tripolitania Area, Libya. Kingdom of Libya, Ministry of Industry, 35 pp.

Miller, H.G. and Singh, V.: 1994, Potential field tilt – a new concept for location of potential field sources. J. Appl. Geophys., 32, 2-3, 213–217. DOI: 10.1016/0926-9851(94)90022-1

Miller, V.C.: 1971, A preliminary investigation of the geomorphology of the Jebel Nefusa. Paper presented at the Symp. Geol. Libya, 365–385.

Ming, Y., Ma, G., Li, L., Han, J. and Wang, T.: 2021, The spatial different order derivative method of gravity and magnetic anomalies for source distribution inversion. Remote Sens., 13, 5, 964. DOI: 10.3390/rs13050964

Nabighian, M.N.: 1972, The analytic signal of two–dimensional magnetic bodies with polygonal cross–section: Its properties and use for automated anomaly interpretation. Geophysics, 37, 3, 507–517. DOI: 10.1190/1.1440276

Narayan, S., Sahoo, S.D., Pal, S., Kumar, U., Pathak, V.K., Majumdar, T. and Chouhan, A.: 2017 Delineation of structural features over a part of the Bay of Bengal using total and balanced horizontal derivative techniques. Geocarto Int., 32, 4, 351–366. DOI: 10.1080/10106049.2016.1140823

Pal, S., Narayan, S., Majumdar, T. and Kumar, U.: 2016 Structural mapping over the 85 E Ridge and surroundings using EIGEN6C4 high–resolution global combined gravity field model: an integrated approach. Mar. Geophys. Res., 37, 3, 159–184. DOI: 10.1007/s11001-016-9274-3

Pal, S.K. and Majumdar, T.: 2015, Geological appraisal over the Singhbhum–Orissa Craton, India using GOCE, EIGEN6–C2 and in situ gravity data. Int. J. Appl. Earth Obs. Geoinf., 35, 96–119. DOI: 10.1016/j.jag.2014.06.007

Reid, A. and Allsop, J.G.H., Millet, A. and Somerton, I.: 1990, Magnetic interpretation in three dimensions using Euler deconvolution. Geophysics, 55, 80–91. DOI: 10.1190/1.1442774

Saadi, N.M., Aboud, E., Saibi, H. and Watanabe, K.: 2008, Integrating data from remote sensing, geology and gravity for geological investigation in the Tarhunah area, Northwest Libya. Int. J. Digit. Earth, 1, 4, 347–366. DOI: 10.1080/17538940802435844

Saadi, N.M., Aboud, E. and Watanabe, K.: 2009, Integration of DEM, ETM+, geologic, and magnetic data for geological investigations in the Jifara Plain, Libya. IEEE Trans. Geosci. Remote Sens., 47,10, 3389–3398. DOI:10.1109/TGRS.2009.2020911

Saadi, N.M., Zaher, M.A., El–Baz, F. and Watanabe, K.: 2011, Integrated remote sensing data utilization for investigating structural and tectonic history of the Ghadames Basin, Libya. Int. J. Appl. Earth Obs. Geoinf., 13, 5, 778–791. DOI: 10.1016/j.jag.2011.05.016

Sadeghi, B., Khalajmasoumi, M., Afzal, P., Moarefvand, P., Yasrebi, A. B., Wetherelt, A. and Ziazarifi, A.: 2013, Using ETM+ and ASTER sensors to identify iron occurrences in the Esfordi 1: 100,000 mapping sheet of Central Iran. J. Afr. Earth Sci., 85, 103–114. DOI: 10.1016/j.jafrearsci.2013.05.003

Saibi, H., Azizi, M. and Mogren, S.: 2016, Structural investigations of Afghanistan deduced from remote sensing and potential field data. Acta Geophys., 64, 4, 978–1003. DOI: 10.1515/acgeo-2016-0046

Spector, A. and Grant, F. S.: 1970, Statistical models for interpreting aeromagnetic data. Geophysics, 35, 2, 293–302. DOI: 10.1190/1.1440092

Steckler, M.S., Berthelot, F., Lyberis, N. and Le Pichon, X.: 1988, Subsidence in the Gulf of Suez: implications for rifting and plate kinematics. Tectonophysics, 153, 1-4, 249–270. DOI:10.1016/0040-1951(88)90019-4

Swire, P. and Gashgesh, T.: 2000, The Bio-Chrono-and Lithostratigraphy and hydrocarbon productivity of the NW Ghadamis Basin and Jifarah Plain. The geology of Northwest Libya. Gutenberg Press, Malta, 1, 173–216.

Tedla, G.E., Van Der Meijde, M., Nyblade, A. and Van der Meer, F.: 2011, A crustal thickness map of Africa derived from a global gravity field model using Euler deconvolution. Geophys. J. Int., 187, 1, 1–9. DOI: 10.1111/j.1365-246X.2011.05140.x

Thompson, D.: 1982, EULDPH: A new technique for making depth estimates from magnetic data computer assisted depth estimates from magnetic data. Geophysics, 47, 31–37. DOI: 10.1190/1.1441278

Trepil, F., Kahoul, S., Uyimwen, O.A., Eshanibli, A., Ismail, N.A., and Ghanoush, H.: 2021, Delineation of structure elements and the basement depth at the Jifara Plain NW Libya using integration application of potential field dataset. Acta Geodyn. Geomater., 18, 1, 83–90. DOI: 10.13168/AGG.2021.0006

Trung, N.N., Lee, S.M. and Que, B.C.: 2004, Satellite gravity anomalies and their correlation with the major tectonic features in the South China Sea. Gondwana Res., 7, 2, 407–424. DOI:10.1016/S1342-937X(05)70793-0

Verduzco, B., Fairhead, J.D., Green, C.M. and MacKenzie, C.: 2004, New insights into magnetic derivatives for structural mapping. Lead. Edge, 23, 2, 116–119. DOI: 10.1190/1.1651454

Zeinelabbdein, K.A., Elmam, M.S., Ali, H.A. and Alhassan, O.M.: 2014, An integrated analysis of Landsat OLI image and satellite gravity data for geological mapping in North Kordofan State, Sudan. J. South Am. Earth Sci., 1, 1, 25–32.

Zivanovic, M.: 1977, Geological Map of Libya. Explanatory Booklet, Sheet Bani Walid NH 33-2. Industrial Research Center, Tripoli, Libya.